Latin American Journal of Solids and Structures
www.lajss.org

Campbell Diagrams of a Spinning Composite Shaft with Curvilinear Fibers

Abstract

This paper presents the vibratory behavior of a spinning composite shaft with curvilinear fibers on rigid bearings in the case of free vibrations. A *p*-version of finite element is used to define the model. A theoretical study allows the establishment of the kinetic energy and the strain energy of the shaft, necessary to the result of the equations of motion. In this model the transverse shear deformation, rotary inertia and gyroscopic effects have been incorporated. A hierarchical beam finite element with six degrees of freedom per node is developed and employed to find the natural frequencies of a spinning composite shaft with variable stiffness (curvilinear fibers). A computer code is elaborate for calculating the natural-frequencies for various rotating speeds of the composite shafts with curvilinear fibers. In the absence of publications of vibration analysis of rotating composite shafts with curvilinear fibers, the formulation is verified by comparisons with published data on rotating composite shafts reinforced by straight fibers. The influence of the physical, geometrical parameters, the boundary conditions and the curvilinear fiber paths on the first natural frequencies of the spinning composite shafts is studied by plotting various Campbell diagrams.

Keywords

Spinning shaft, composite materials, curvilinear fibers, variable stiffness, *p*- version, finite element method, Campbell diagram.

Abdelkrim Boukhalfa

Computational mechanics research laboratory, Department of mechanical engineering, Faculty of technology, University of Tlemcen, 13000, Algeria.

Author e-mail: BKA1975E@Yahoo.fr

http://dx.doi.org/10.1590/1679-78253326

Received 27.08.2016
In revised form 19.01.2017
Accepted 23.01.2017
Available online 26.01.2017

1 INTRODUCTION

Rotating machines such as pumps, turbines, compressors, etc. have become indispensable elements for modern industry. Manufacturers are encouraged to improve their products. Advances in the design and manufacture allow today to increase both the performance and efficiency of the machines by making them operate in speed ranges increasingly high. However, the forces generated, increasingly important, strongly urge the overall dynamic behavior of the machine and the vibration am-

plitudes often become too high for the structure can withstand. For this, the amplitude of deformation of the shaft must be controlled and its resonance frequencies known to avoid that too much vibration generates a lower return, too much noise, ...; and this vibration can even lead to instability and damage to the system: fatigue fracture, damage to the bearings, rotor/stator friction. The study of the dynamics of rotating machines is more relevant than ever.

The appearance of composite materials has opened new paths for increasing the performance of industrial machines (automotive, aeronautics and space sectors) because of their intrinsic qualities such as lightness (associated with high strength characteristics) and good resistance to corrosion. The field of use of machines has grown through development of new materials, developed using new methods of design and manufacturing.

Various research works (DiNardo and Lagace, 1989; Leissa and Martin, 1990; Hyer and Charette, 1991; Hyer and Lee, 1991; Waldhart, 1996) on composite materials is concluded that it is feasible to improve the mechanical properties of composite structures by changing the fiber orientation angle around areas of high stress concentration. This modification in alignment of the fibers results in a local change of the stiffness which results in an overall change of the rigidity of a composite structure. This variation is the origin of the name of this new construction of composite materials, is the composite materials with variable stiffness (Gürdal and Olmedo, 1992; Olmedo and Gürdal, 1993; Gürdal and Olmedo, 1993; Tatting, 1998; Gürdal et al., 2005). The development of this new concept of manufacture of composite materials was made possible thanks to the evolution of AFP technology, Automated Fiber Placement process (Marouene, 2015).

Several examples of research works on the design and optimization of composite materials have demonstrated the potential of the variable-stiffness design to improve the in-plane stiffness (Gürdal and Olmedo, 1993; Nik et al., 2012), buckling resistance (Hyer and Lee, 1991; Wu et al., 2013), strength (Lopes et al., 2008; Khani et al., 2011), vibration response (Abdalla et al., 2007; Blom et al., 2008; Ribeiro and Akhavan, 2012; Ribeiro et al., 2014; Ribeiro, 2015a-b; Yazdani et Ribeiro, 2015; Venkatachari et al., 2016) and bending properties (Blom et al.,2010; Rouhi et al. ,2015).

Few studies on the vibratory behavior of beams with curvilinear fibers are presented in literature. Zamani et al. (2011) published an investigation of the possible performance improvements of thin walled composite beams through the use of the variable stiffness concept with curvilinear fiber. In the same axis, Haddadpour and Zamani (2012) presented the aeroelastic design of composite wings.

Because of lack of publications in the case of composite rotor dynamics with curvilinear fibers (variable stiffness), our contribution has come to fill this gap. Mastering vibration behavior of composite rotors with curvilinear fibers requires knowledge of their dynamic characteristics. The prediction of this knowledge is fundamental in the design of future rotating machinery to provide a clear idea of secure band of rotating speeds. In the presented spinning composite shafts with curvilinear fibers, the Timoshenko beam theory will be adopted. It is the purpose of the present work to study vibratory behaviors such as natural frequencies of the spinning shaft by plotting of the Campbell diagrams (variation of the bending frequencies according to the rotating speeds). In this model, the transverse shear deformation, rotary inertia, and gyroscopic effects have been incorporated. To determine the spinning shaft system's responses, the *p*-version of finite element method with trigono-

metric shape functions (Boukhalfa et al., 2008; Boukhalfa, 2014) is used here to approximate the governing equations by a system of ordinary differential equations.

2 EQUATIONS OF MOTION

2.1 Kinetic and Strain Energy Expressions of the Shaft

The shaft is modelled as a Timoshenko beam, i.e., first order shear deformation theory with rotary inertia and gyroscopic effect is used. The shaft rotates at constant speed about its longitudinal axis. Due to the presence of fibers oriented than axially or circumferentially, coupling is made between bending and twisting. The shaft has a uniform, circular cross section.

The following displacement field of a spinning shaft is assumed by choosing the coordinate axis x to coincide with the shaft axis:

$$\begin{cases} U(x,y,z,t) = U_0(x,t) + z\beta_x(x,t) - y\beta_y(x,t) \\ V(x,y,z,t) = V_0(x,t) - z\phi(x,t) \\ W(x,y,z,t) = W_0(x,t) + y\phi(x,t) \end{cases} \tag{1}$$

Where U, V and W are the flexural displacements of any point on the cross-section of the shaft in the x, y and z directions. The variables U_0, V_0 and W_0 are the flexural displacements of the shaft's axis while β_x and β_y are the rotation angles of the cross-section, about the y and z axis respectively. The ϕ is the angular displacement of the cross-section due to the torsion deformation of the shaft (see Figure 1).

The various components of strain energy come from the shaft (Boukhalfa et al., 2008):

$$E_d = \frac{1}{2}\int_0^L A_{11}\left(\frac{\partial U_0}{\partial x}\right)^2 dx + \frac{1}{2}\int_0^L B_{11}\left[\left(\frac{\partial \beta_x}{\partial x}\right)^2 + \left(\frac{\partial \beta_y}{\partial x}\right)^2\right]dx + \frac{1}{2}k_s\int_0^L B_{66}\left(\frac{\partial \phi}{\partial x}\right)^2 dx + \frac{1}{2}k_s\int_0^L A_{16}\left[2\frac{\partial \phi}{\partial x}\frac{\partial U_0}{\partial x} + \beta_y\frac{\partial \beta_x}{\partial x} - \beta_x\frac{\partial \beta_y}{\partial x} - \frac{\partial V_0}{\partial x}\frac{\partial \beta_x}{\partial x} - \frac{\partial W_0}{\partial x}\frac{\partial \beta_y}{\partial x}\right]dx + \frac{1}{2}k_s\int_0^L (A_{55}+A_{66})\left[\left(\frac{\partial V_0}{\partial x}\right)^2 + \left(\frac{\partial W_0}{\partial x}\right)^2 + \beta_x^2 + \beta_y^2 + 2\beta_x\frac{\partial W_0}{\partial x} - 2\beta_y\frac{\partial V_0}{\partial x}\right]dx \tag{2}$$

Where

$$\begin{cases} A_{11} = \pi\sum_{n=0}^{k} C'_{11n}(R_{n+1}^2 - R_n^2)\,;\; A_{55} = \frac{\pi}{2}\sum_{n=0}^{k} C'_{55n}(R_{n+1}^2 - R_n^2)\,;\; A_{66} = \frac{\pi}{2}\sum_{n=0}^{k} C'_{66n}(R_{n+1}^2 - R_n^2) \\ A_{16} = \frac{2\pi}{3}\sum_{n=0}^{k} C'_{16n}(R_{n+1}^3 - R_n^3)\,;\; B_{11} = \frac{\pi}{4}\sum_{n=0}^{k} C'_{11n}(R_{n+1}^4 - R_n^4)\,;\; B_{66} = \frac{\pi}{2}\sum_{n=0}^{k} C'_{66n}(R_{n+1}^4 - R_n^4) \end{cases} \tag{3}$$

Where k is the number of the layer, R_n is the nth layer inner radius of the composite shaft and R_{n+1} it is the nth layer outer of the composite shaft. L is the length of the composite shaft. k_s is the shear correction factor proposed by Dharmarajan and McCutchen (1973). And C_{ij}' are the effective elastic constants, they are related to lamination angle η and the elastic constants of principal axes of composite lamina (Berthelot, 1996).

$$\begin{cases} C'_{11} = C_{11}\cos^4\eta + C_{22}\sin^4\eta + 2(C_{12}+2C_{66})\sin^2\eta\cos^2\eta \\ C'_{16} = (C_{11}-C_{12}-2C_{66})\sin\eta\cos^3\eta + (C_{12}-C_{22}+2C_{66})\sin^3\eta\cos\eta \\ C'_{66} = [C_{11}+C_{22}-2(C_{12}+C_{66})]\sin^2\eta\cos^2\eta + C_{66}(\sin^4\eta+\cos^4\eta) \\ C'_{55} = C_{44}\sin^2\eta + C_{55}\cos^2\eta \end{cases} \tag{4}$$

The kinetic energy of the spinning composite shaft (Boukhalfa et al., 2008), upon including the effects of translatory and rotary inertia, it can be written as

$$E_c = \frac{1}{2}\int_0^L \left[I_m\left(\dot{U}_0^2 + \dot{V}_0^2 + \dot{W}_0^2\right) + I_d\left(\dot{\beta}_x^2 + \dot{\beta}_y^2\right) - 2\Omega I_p\beta_x\dot{\beta}_y + 2\Omega I_p\dot{\phi} + I_p\dot{\phi}^2 + \Omega^2 I_p + \Omega^2 I_d\left(\beta_x^2 + \beta_y^2\right)\right] dx \tag{5}$$

Where Ω is the rotating speed of the shaft which is assumed constant and ρ_n is the density of the nth layer of the composite shaft. The $2\Omega I_p\beta_x\dot{\beta}_y$ term accounts for the gyroscopic effect, and $I_d\left(\dot{\beta}_x^2 + \dot{\beta}_y^2\right)$ represents the rotary inertia effect. The mass moments of inertia I_m, the diametrical mass moments of inertia I_d and polar mass moment of inertia I_p of spinning shaft per unit length are defined in equation (6). As the $\Omega^2 I_d\left(\beta_x^2 + \beta_y^2\right)$ term is far smaller than $\Omega^2 I_p$, it will neglected in further analysis.

$$I_m = \pi\sum_{n=0}^{k}\rho_n\left(R_{n+1}^2 - R_n^2\right), I_d = \frac{\pi}{4}\sum_{n=0}^{k}\rho_n\left(R_{n+1}^4 - R_n^4\right), I_p = \frac{\pi}{2}\sum_{n=0}^{k}\rho_n\left(R_{n+1}^4 - R_n^4\right) \tag{6}$$

2.2 Variable-Stiffness Definitions

As showed in Figure 2, a typical curvilinear fiber starting from an arbitrary reference point with a fiber orientation angle T_0 and moving along the x axis, until the fiber orientation angle reaches a value T_1 at a characteristic distance L from the reference point. With linear fiber orientation variation derived and used by Gürdal and Olmedo (1993), the path definition formulated as

$$\eta(x) = T_0 + (T_1 - T_0)(x/L) \tag{7}$$

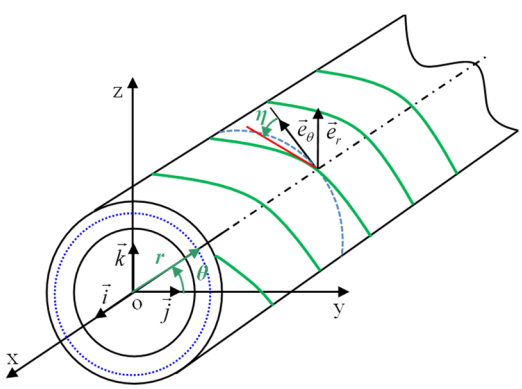

Figure 1: The geometry of a composite shaft.

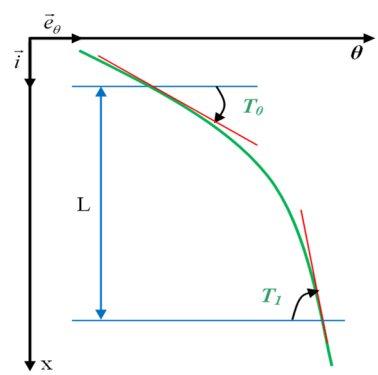

Figure 2: Path definition of variable stiffness laminate.

In which η denotes the ply-angle measured from the positive θ-axis toward the positive x-coordinate in Figure 2. Using this definition, the vector of design variables is $T^{(n)} =< T_0^{(n)} | T_1^{(n)} >$ Where T_0 and T_1 are the fiber orientation angle at the root and tip cross sections which can have values between 0° and 180°. So the two design variables in each layer n are required to determine the variation of the fiber orientation on the surface of the shaft. Therefore the equation (4) becomes as follows:

$$\begin{cases} C'_{11} = C_{11}\cos^4\eta(x) + C_{22}\sin^4\eta(x) + 2(C_{12}+2C_{66})\sin^2\eta(x)\cos^2\eta(x) \\ C'_{16} = (C_{11}-C_{12}-2C_{66})\sin\eta(x)\cos^3\eta(x) + (C_{12}-C_{22}+2C_{66})\sin^3\eta(x)\cos\eta(x) \\ C'_{66} = [C_{11}+C_{22}-2(C_{12}+C_{66})]\sin^2\eta(x)\cos^2\eta(x) + C_{66}(\sin^4\eta(x)+\cos^4\eta(x)) \\ C'_{55} = C_{44}\sin^2\eta(x) + C_{55}\cos^2\eta(x) \end{cases} \tag{8}$$

2.3 Hierarchical Beam Element Formulation

The spinning flexible shaft is descretized by one hierarchical beam element with two nodes 1 and 2. The element's nodal degrees of freedom at each node are U_0 , V_0 , W_0 , β_x , β_y and ϕ. The local and non-dimensional co-ordinates are related by $\xi = x/L$ with $\xi \in [0,1]$.

The vector displacement formed by the variables U_0 , V_0 , W_0 , β_x , β_y and ϕ can be written as

$$\begin{aligned} &U_0 = [N_U]\{q_U\} = \sum_{m=1}^{p_U} x_m(t)\cdot f_m(\xi), V_0 = [N_V]\{q_V\} = \sum_{m=1}^{p_V} y_m(t)\cdot f_m(\xi), W_0 = [N_W]\{q_W\} = \sum_{m=1}^{p_W} z_m(t)\cdot f_m(\xi), \\ &\beta_x = [N_{\beta_x}]\{q_{\beta_x}\} = \sum_{m=1}^{p_{\beta_x}} \beta_{xm}(t)\cdot f_m(\xi), \beta_y = [N_{\beta_y}]\{q_{\beta_y}\} = \sum_{m=1}^{p_{\beta_y}} \beta_{ym}(t)\cdot f_m(\xi), \phi = [N_\phi]\{q_\phi\} = \sum_{m=1}^{p_\phi} \phi_m(t)\cdot f_m(\xi) \end{aligned} \tag{9}$$

And

$$[N_{U,V,V,\beta_x,\beta_y,\phi}] = [f_1\ f_2 \ldots\ldots f_{p_U,p_V,p_W,p_{\beta_x},p_{\beta_y},p_\phi}] \tag{10}$$

Where p_U , p_V , p_W , p_{β_x} , p_{β_y} and p_ϕ are the numbers of hierarchical terms of displacements (are the numbers of shape functions of displacements). In this work, $p_U = p_V = p_W = p_{\beta_x} = p_{\beta_y} = p_\phi = p$

The vector of generalized coordinates given by

$$\{q\} = \{ q_U, q_V, q_W, q_{\beta_x}, q_{\beta_y}, q_\phi \}^T \tag{11}$$

Where

$$\begin{aligned} &\{q_U\} = \{x_1, x_2, x_3, ..., x_{p_U}\}^T \exp(j\omega t), \{q_V\} = \{y_1, y_2, y_3, ..., y_{p_V}\}^T \exp(j\omega t), \\ &\{q_W\} = \{z_1, z_2, z_3, ..., y_{p_W}\}^T \exp(j\omega t), \{q_{\beta_x}\} = \{\beta_{x_1}, \beta_{x_2}, \beta_{x_3}, ..., \beta_{x_{p_{\beta_x}}}\}^T \exp(j\omega t), \\ &\{q_{\beta_y}\} = \{\beta_{y_1}, \beta_{y_2}, \beta_{y_3}, ..., \beta_{y_{p_{\beta_y}}}\}^T \exp(j\omega t), \{q_\phi\} = \{\phi_1, \phi_2, \phi_3, ..., \phi_{p_\phi}\}^T \exp(j\omega t) \end{aligned} \tag{12}$$

The group of the shape functions used in this study (Boukhalfa et al., 2008; Boukhalfa, 2014) is

$$\left\{f_1 = 1-\xi\,, f_2 = \xi\,, f_{r+2} = \sin\left(\delta_r\ \xi\right); \delta_r = r\pi\ \ ;\ \ r = 1\,,2\,,3\,,....\right\} \tag{13}$$

The functions (f_1, f_2) are those of the finite element method necessary to describe the nodal displacements of the element; whereas the trigonometric functions f_{r+2} contribute only to the internal field of displacement and do not affect nodal displacements. The most attractive particularity of the trigonometric functions is that they offer great numerical stability. The shaft is modeled by one element called hierarchical finite element with p shape functions.

By modelling of the spinning composite shaft by the p- version of the finite element method and applying the Euler-Lagrange equations, the equations of motion of free vibration of spinning flexible shaft can be obtained.

$$[M]\{\ddot{q}\} + [G]\{\dot{q}\} + [K]\{q\} = \{0\} \tag{14}$$

$[M]$ and $[K]$ are the mass and stiffness matrix, $[G]$ is the gyroscopic matrix. The different matrices of the system of equation are given in Appendix.

3 NUMERICAL RESULTS

In this work, we expose the results obtained by our computer code for various applications. Convergence towards the solutions is studied by increasing the numbers of shape functions of displacements. In the absence of data on vibrations of spinning composite shafts with curvilinear fibers, the formulation is verified by comparisons with published data on spinning composite shafts reinforced by straight fibers. A study of the influence of mechanical and geometrical parameters, boundary conditions and the curvilinear fiber paths on the natural frequencies of the spinning composite shafts with variable stiffness. After the convergence study, in all studied examples, we takes p =10.

3.1 Convergence

The mechanical properties of boron-epoxy are (Bert and Kim, 1995) E_{11} = 211.0 GPa, E_{22} = 24.1 GPa, G_{12} = G_{23} = 6.9 GPa, ν_{12} = 0.36, ρ = 1967.0 Kg/m^3. The shaft has a total length L of 2.47 m. The mean diameter D and the wall thickness e of the shaft are 12.69 cm and 1.321 mm respectively. The shaft has three layers of equal thickness with curvilinear fibers [<15°|30°>,<45°|60°>,<75°|90°>] starting from the inside surface of the hollow shaft. A shear correction factor k_s of 0.503 is also used and the rotating speed Ω =0. In this example, the boron - epoxy spinning shaft is modeled by one element of length L.

The results of the three bending modes for various boundary conditions of the composite shaft with variable stiffness as a function of the number of hierarchical terms p are shown in Figure 3. Figure clearly shows that rapid convergence from above to the solutions occurs as the number of hierarchical terms is increased. This shows the exactitude of the method even with one element and a reduced number of the shape functions. It is noticeable in the case of low frequencies, a very small p is needed (p =5 sufficient), whereas in the case of the high frequencies, and in order to have a good convergence, p should be increased.

3.2 Validation

In the absence of publications of vibration analysis of spinning composite shafts with curvilinear fibers, this model is validated by calculating the critical speeds of spinning composite shafts with straight fibers.

In the following example already treated in our publication (Boukhalfa et al., 2008), the critical speeds of composite shaft for different lamination angles η are analysed and compared with those available in the literature to verify the present model. In this example, the composite hollow shaft made of graphite-epoxy laminae, which are considered by Bert and Kim (1995), are investigated. The mechanical and geometrical properties of this shaft are: $E_{11} = 139.0$ GPa, $E_{22} = 11.0$ GPa, $G_{12} = 6.05$ GPa, $G_{23} = 3.78$ GPa , $\nu_{12} = 0.313$, $\rho = 1578.0$ Kg/m^3, $L = 2.47$ m, $D = 12.69$ cm, $e = 1.321$ mm, 10 layers with straight fibers $[90°/45°/\text{-}45°/0°_6/90°]$ of equal thickness starting from the inside surface of the hollow shaft, $k_s = 0.503$.

The shaft is modeled by one element. The shaft is simply-supported at the ends. In this validation, $p = 10$. The results are listed in Table 1. The results from the present model are compatible to that of continuum based Timoshenko beam theory of Chang et al. (2004). In this reference, the supports are flexible and the shaft is modeled by 20 finite elements of equal length (h-version of finite element method (FEM)). But in our application the supports are rigid and the shaft is modeled by only one element with two nodes. In this example, is not noticeable the difference between shaft bi-supported on rigid supports or elastic supports because the stiffness of the supports are very large, 1740 GN/m for each support. The rapid convergence while taking only one element and a reduced number of shape functions shows the advantage of the method used. We should stress here that the present model is not only applicable to the thin-walled composite shafts as studied above, but also to the thick-walled shafts as well as to the solid ones.

	Theory or Method	Lamination angle η [°]						
		0	15	30	45	60	75	90
Bert and Kim (1995)	Sanders shell.	5527	4365	3308	2386	2120	2020	1997
	Bernoulli- Euler beam.	6425	5393	4269	3171	2292	1885	1813
	Bresse-Timoshenko beam.	6072	5209	4197	3143	2278	1874	1803
Chang et al. (2004)	Continuum based Timoshenko beam by the h-version of FEM.	6072	5331	4206	3124	2284	1890	1816
Present	Timoshenko beam by the p- version of FEM.	6094	5359	4222	3129	2284	1890	1816

Table 1: Critical speeds [rpm] of the graphite-epoxy shaft for various lamination angles.

3.3 Results and Discussions

3.3.1 Influence of Gyroscopic Effect on the Natural Frequencies

In this example, the natural frequencies of a boron- epoxy spinning shaft are analysed. The orientation of fibers in the various layers, the mechanical and geometrical properties are the same as those of the first shaft used in convergence study. The Campbell diagram for the first bending mode of

the boron- epoxy spinning shaft for different boundary conditions is shown in Figure 4. The Campbell diagram for the first three bending modes of the boron- epoxy spinning shaft bi- simply supported (S-S) is shown in Figure 5.

The gyroscopic effect inherent to spinning structures induces a precession motion. The forward modes (F) increase with increasing rotating speed however the backward modes (B) decrease. This effect has a significant influence on the behaviors of the spinning shafts. The numerical results of these figures are given in tables 2 and 3 to show this influence of the gyroscopic effect.

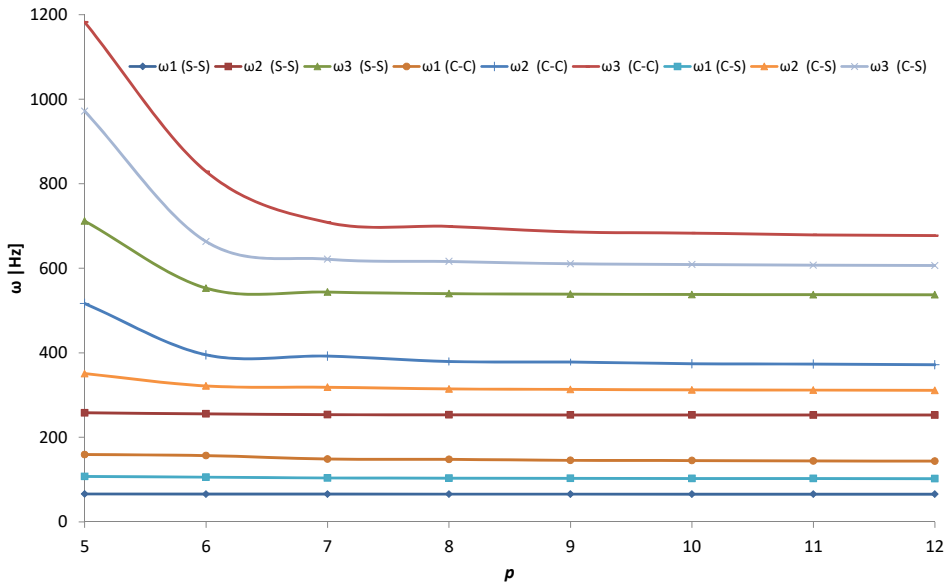

Figure 3: Convergence of the natural frequency ω for the three bending modes of the boron-epoxy shaft with variable stiffness [<15°|30°>,<45°|60°>,<75°|90°>] for different boundary conditions (S: simply-supported; C: clamped) as a function of the number of hierarchical terms p.

Rotating speed Ω [rad/s]	Frequency ω_1 [Hz]					
	1B (S-S)	1F (S-S)	1B (C-C)	1F (C-C)	1B (C-S)	1F (C-S)
0	65.6539	65.6539	145.1298	145.1298	102.6872	102.6872
100	65.6046	65.7032	145.0773	145.1822	102.6320	102.7425
200	65.5554	65.7525	145.0249	145.2347	102.5767	102.7978
300	65.5062	65.8018	144.9725	145.2872	102.5215	102.8532
400	65.4571	65.8512	145.3397	145.3397	102.4663	102.9085
500	65.4080	65.9006	144.8676	145.3921	102.4111	102.9639
600	65.3589	65.9501	144.8152	145.4446	102.3559	103.0193
700	65.3098	65.9996	144.7628	145.4971	102.3008	103.0747
800	65.2608	66.0491	144.7104	145.5497	102.2457	103.1301
900	65.2118	66.0986	144.6580	145.6022	102.1906	103.1855
1000	65.1629	66.1482	144.6056	145.6547	102.1355	103.2410

Table 2: The first bending mode of the boron- epoxy shaft with variable stiffness [<15°|30°>,<45°|60°>,<75°|90°>] for different boundary conditions and various rotating speed Ω (S: simply-supported; C: clamped).

Rotating speed Ω [rad/s]	Frequency ω [Hz]					
	1B (S-S)	1F (S-S)	2B (S-S)	2F (S-S)	3B (S-S)	3F (S-S)
0	65.6539	65.6539	252.9123	252.9123	537.8773	537.8773
100	65.6046	65.7032	252.7413	253.0835	537.5647	538.1899
200	65.5554	65.7525	252.5703	253.2547	537.2522	538.5026
300	65.5062	65.8018	252.3993	253.4260	536.9397	538.8152
400	65.4571	65.8512	252.2284	253.5974	536.6272	539.1279
500	65.4080	65.9006	252.0577	253.7688	536.3147	539.4407
600	65.3589	65.9501	251.8869	253.9403	536.0022	539.7534
700	65.3098	65.9996	251.7163	254.1119	535.6898	540.0662
800	65.2608	66.0491	251.5457	254.2835	535.3774	540.3790
900	65.2118	66.0986	251.3752	254.4552	535.0651	540.6918
1000	65.1629	66.1482	251.2048	254.6270	534.7528	541.0046

Table 3: The first three of bending modes of the boron- epoxy shaft bi- simply supported (S-S) with variable stiffness [<15°|30°>,<45°|60°>,<75°|90°>] for different rotating speed Ω.

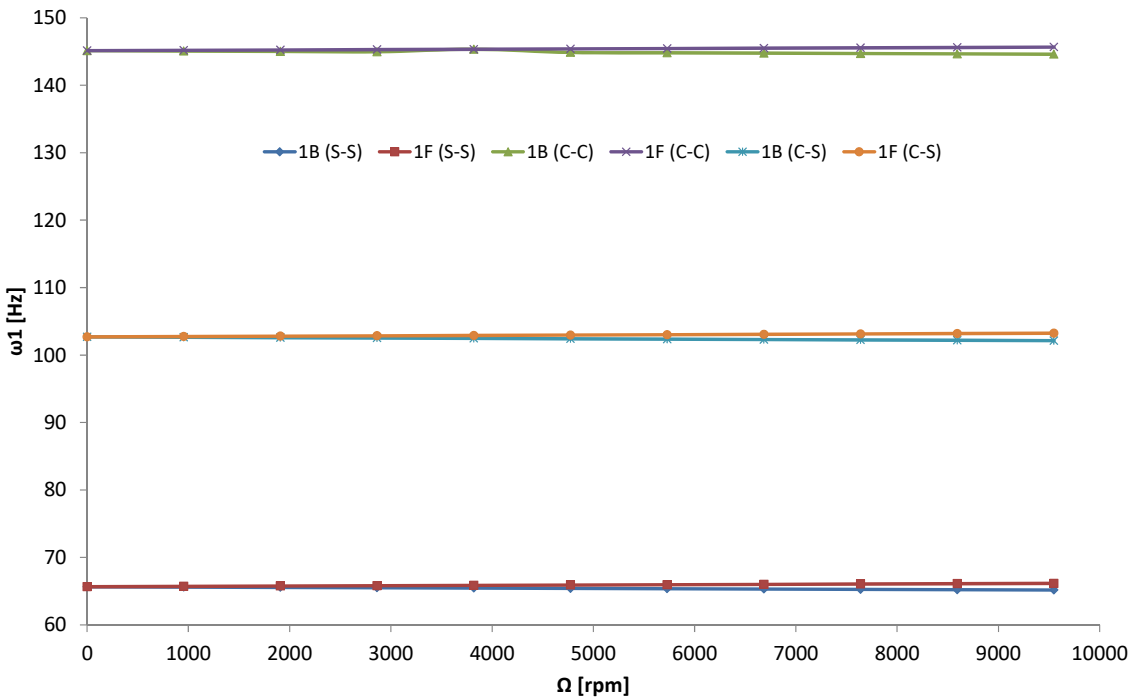

Figure 4: Campbell diagram for the first bending mode of the boron- epoxy shaft with variable stiffness [<15°|30°>,<45°|60°>,<75°|90°>] for different boundary conditions (S: simply-supported; C: clamped).

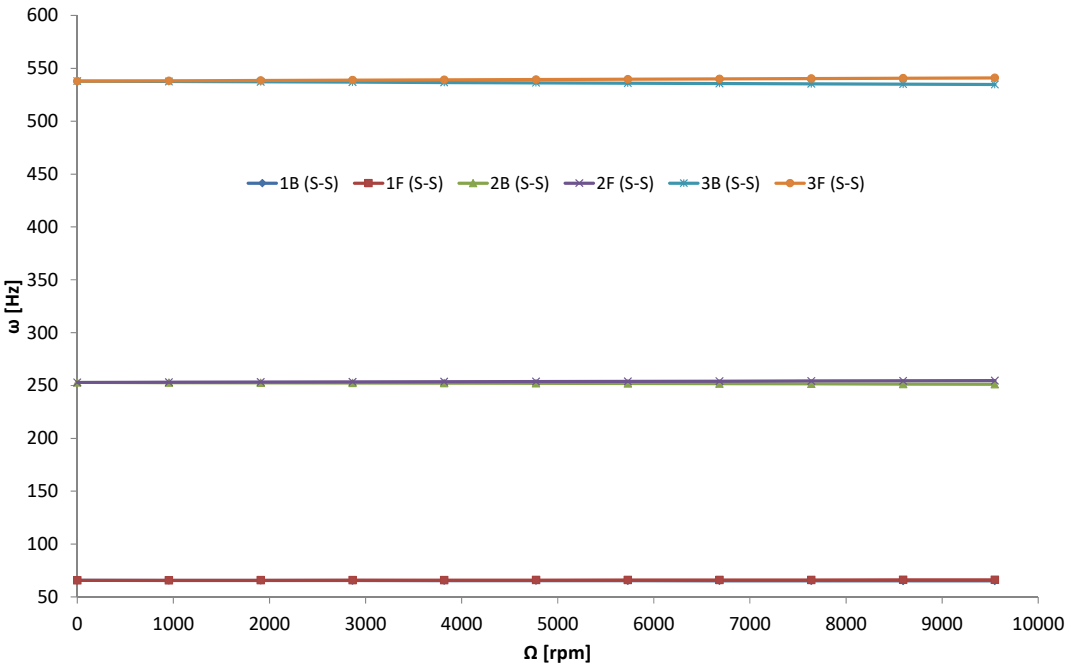

Figure 5: Campbell diagram for the first three of bending modes of the boron- epoxy shaft bi- simply supported (S-S) with variable stiffness [<15°|30°>,<45°|60°>,<75°|90°>].

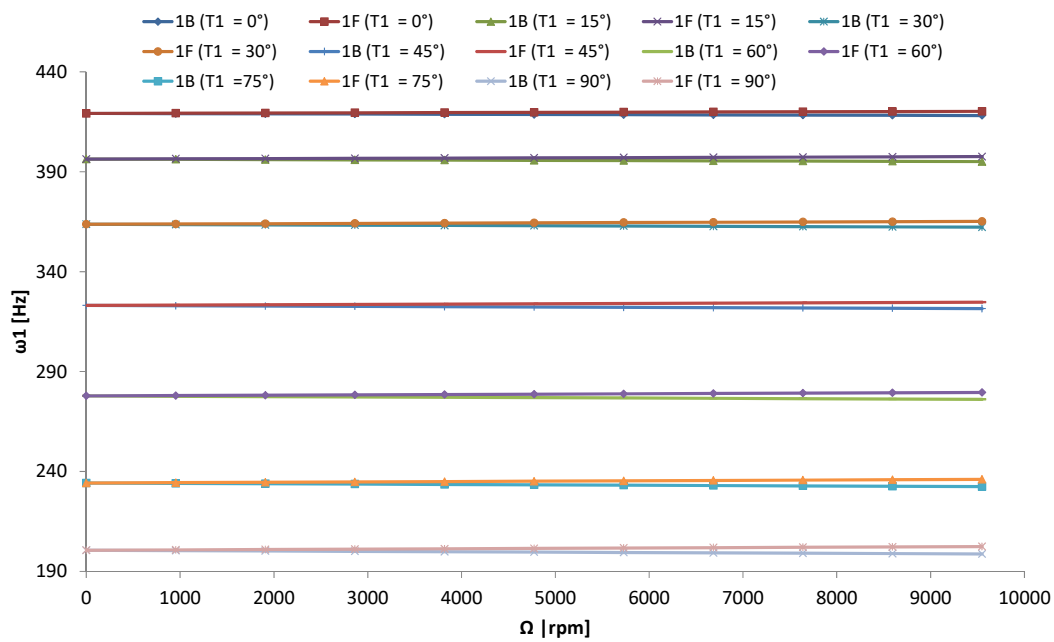

Figure 6: Campbell diagram for the bending fundamental frequency ω_1 of the carbon- epoxy shaft with variable stiffness $[<15^{\circ}|T_1^{\circ}>]$ bi-simply supported.

3.3.2. Influence of the fibers orientations on the natural frequencies

In order to show the effects of the fibers orientations on the natural frequencies, a carbon-epoxy spinning shafts are bi- simply-supported (S-S). The physical properties of material (Singh and Gupta, 1996) are: $E_{11} = 130.$ GPa, $E_{22} = 10.$ GPa, $G_{12} = G_{23} = 7.$ GPa, $\nu_{12} = 0.25$, $\rho = 1500.$ Kg/m^3. The geometric parameters are L =1.0 m, $D = 0.1$ m, $e = 4$ mm, single layer with curvilinear fibers [$<T_0|T_1>$], and $k_s = 0.503$. We fix T_0 =15° and we change T_1.

Figure 6 shows the variation of the bending fundamental frequency ω_1 according to the rotating speeds Ω for various curvilinear fibers [$<15^{\circ}|T_1>$]. According to these results, the first bending frequencies of the composite shaft decrease when T_1 angle increases and vice versa.

3.3.3 Influence of the stacking sequence on the natural frequencies

By considering the same preceding carbon- epoxy spinning shaft but we change the fiber orientations. In order to show the permutation effects of the fibers orientations on the natural frequencies, we consider the following permutations for one and two then for three layers of equal thickness starting from the inside surface of the hollow shaft:

- First permutation between two angles for single curvilinear fibers in the same layer to have [<15°|75°>] and [<75°|15°>];
- Second permutation between two curvilinear fibers to have [<15°|75°>,[<45°|60°>] and [<45°|60°>,[<15°|75°>];
- Third permutation between three curvilinear fibers to have [<15°|75°>,<45°|60°>,<30°|90°>] , [<45°|60°>,<15°|75°>,<30°|90°>] and [<30°|90°>,<45°|60°>,<15°|75°>].

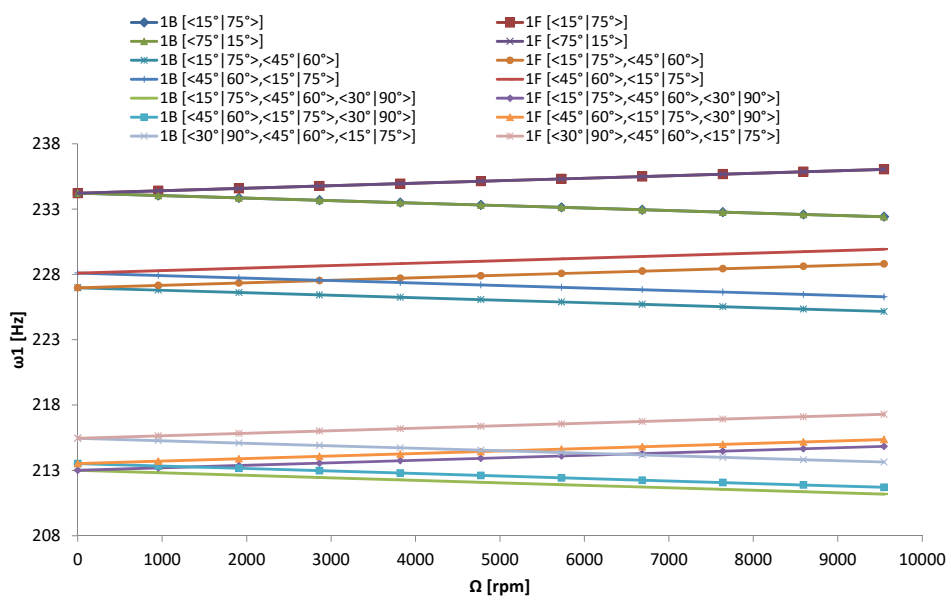

Figure 7: Campbell diagram for the bending fundamental frequency ω_1 of the carbon- epoxy shaft with variable stiffness bi-simply supported for different permutations of fiber orientations.

Figure 7 shows the Campbell diagram for the bending fundamental frequency of the carbon-epoxy shaft bi-simply supported (S-S) with variable stiffness for different permutations of fiber orientations.

It is found that the first natural frequencies are almost the same if we permute the angles T_0 and T_1 in the same layer [$<T_0|\ T_1>$] and [$<T_1|\ T_0>$].

It is found that the first natural frequencies are very close if we permute two adjacent layers:

- [$<T_0^1|T_1^1>$, $<T_0^2|T_1^2>$] and [$<T_0^2|T_1^2>$, $<T_0^1|T_1^1>$] for two layers;
- [$<T_0^1|T_1^1>$, $<T_0^2|T_1^2>$,$<T_0^3|T_1^3>$] and [$<T_0^2|T_1^2>$, $<T_0^1|T_1^1>$,$<T_0^3|T_1^3>$] for three layers.

In order to show the symmetric, anti-symmetric and unsymmetric effects of the fibers orientations on the natural frequencies, we consider the following stackings for three then for four layers of equal thickness starting from the inside surface of the hollow shaft.

➢ For three layers, we use three fiber orientations <30°|60°>,<45°|60°> and -<45°|60°> to combine various stackings:

- Two symmetric lay-up [<45°|60°>,<30°|60°>,<45°|60°>] and [<30°|60°>, <45°|60°>,<30°|60°>];
- Two anti-symmetric lay-up [-<45°|60°>,<30°|60°>,<45°|60°>] and [<45°|60°>,<30°|60°>,-<45°|60°>];
- Two unsymmetric lay-up [<45°|60°>,<45°|60°>,<30°|60°>] and [<30°|60°>,<30°|60°>,<45°|60°>].

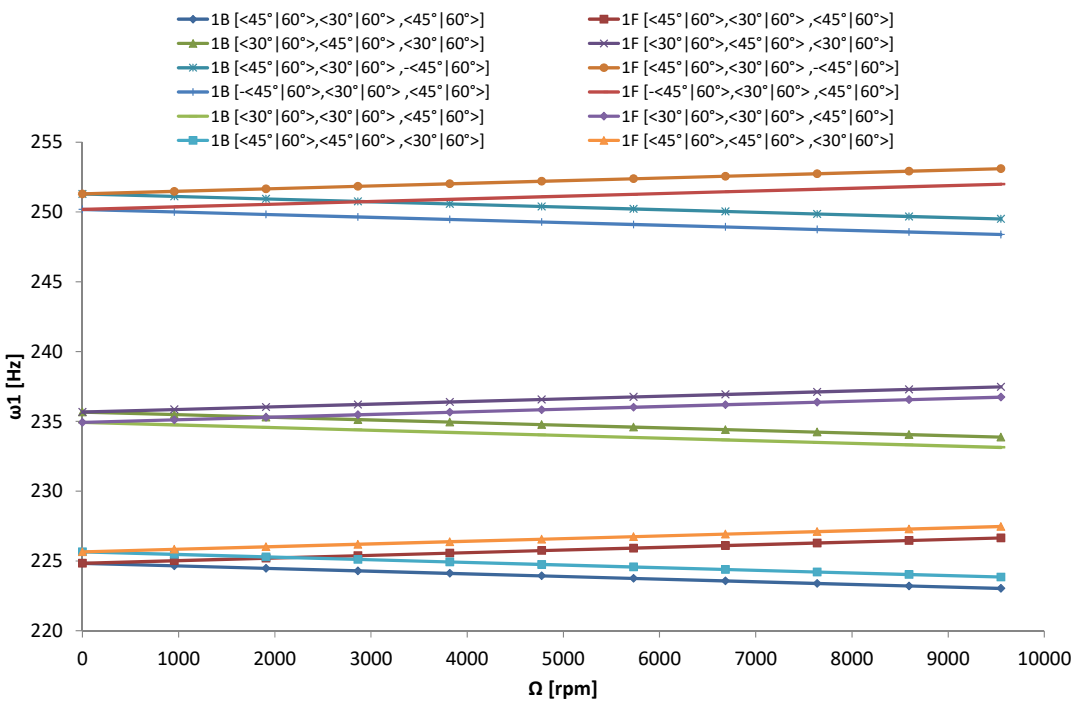

Figure 8: Campbell diagram for the bending fundamental frequency ω_1 of the carbon- epoxy shaft bi-simply supported with symmetric, anti-symmetric and unsymmetric stackings (three layers).

Figure 8 shows the Campbell diagram for the bending fundamental frequency ω_1 of the carbon-epoxy shaft bi-simply supported (S-S) with symmetric, anti-symmetric and unsymmetric stackings for three layers.

It is found that the first natural frequencies of spinning shafts which have anti-symmetric stackings are very close [-$<T_0^1|T_1^1>$, $<T_0^2|T_1^2>$,$<T_0^1|T_1^1>$] and [$<T_0^1|T_1^1>$, $<T_0^2|T_1^2>$,-$<T_0^1|T_1^1>$].

It is found that the first natural frequencies of spinning shafts which have symmetric stackings are a little close [$<T_0^1|T_1^1>$, $<T_0^2|T_1^2>$,$<T_0^1|T_1^1>$] and [$<T_0^2|T_1^2>$, $<T_0^1|T_1^1>$,-$<T_0^2|T_1^2>$].

- For four layers, we use three fiber orientations <15°|30°>,-<15°|30°>,-<45°|60°> and <45°|60°> to combine various stackings:
  - Two symmetric lay-up [<15°|30°>,<45°|60°>,<45°|60°>,<15°|30°>] and [-<15°|30°>,<45°|60°>,<45°|60°>,-<15°|30°>];
  - Two anti-symmetric lay-up [-<15°|30°>,-<45°|60°>,<45°|60°>,<15°|30°>] and [-<15°|30°>,<45°|60°>,-<45°|60°>,<15°|30°>];
  - Two unsymmetric lay-up [<15°|30°>, <15°|30°>,<45°|60°>, <45°|60°>] and [<15°|30°>,-<15°|30°>,<45°|60°>,-<45°|60°>].

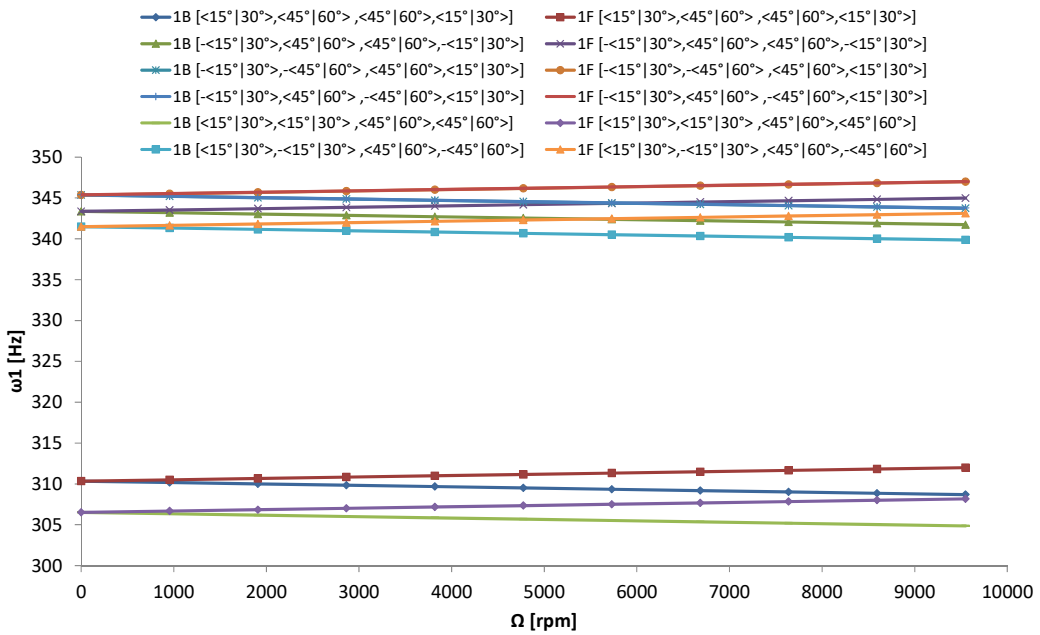

Figure 9: Campbell diagram for the bending fundamental frequency ω_1 of the carbon- epoxy shaft bi-simply supported with symmetric, anti-symmetric and unsymmetric stackings (four layers).

Figure 9 shows the Campbell diagram for the bending fundamental frequency ω_1 of the carbon-epoxy shaft bi-simply supported (S-S) with symmetric, anti-symmetric and unsymmetric stackings for four layers.

It is found that the first natural frequencies of spinning shafts which have anti-symmetric stackings are very close [$<T_0^1|T_1^1>$, $<T_0^2|T_1^2>$, $<T_0^2|T_1^2>$,$<T_0^1|T_1^1>$] and [-$<T_0^1|T_1^1>$, $<T_0^2|T_1^2>$,$<T_0^2|T_1^2>$,-$<T_0^1|T_1^1>$].

It is found that the first natural frequencies of spinning shafts which have symmetric stackings are a little close $[-<T_0^1|T_1^1>, -<T_0^2|T_1^2>,<T_0^2|T_1^2>,<T_0^1|T_1^1>]$ and $[-<T_0^1|T_1^1>, <T_0^2|T_1^2>,-<T_0^2|T_1^2>,<T_0^1|T_1^1>]$.

It is found that the first natural frequencies of spinning shafts which have unsymmetric stackings are far.

3.3.4 Influence of the Ratios *L/D* and *e/D* on the Natural Frequencies

In Figure 10, the variation of the bending fundamental frequency ω_1 of the carbon-epoxy shaft bi-simply supported as a function of rotating speed Ω (Campbell diagram) for various ratios L/D. It is the same spinning shaft used previously but we change the fiber orientations at six layers of equal thickness with curvilinear fibers $[\mp<15°|75°>,\mp<45°|60°>,\mp<30°|90°>]$ i.e. $[-<15°|75°>,+<15°|75°>, -<45°|60°>,+<45°|60°>, -<30°|90°>,+<30°|90°>]$ starting from the inside surface of the hollow shaft (L =1m).

It is noted, if ratio L/D increases the first natural frequencies decreases and vice versa. For more details you can see our publication (Boukhalfa and Hadjoui, 2010).

In Figure 11, the variation of the bending fundamental frequency ω_1 of the carbon-epoxy spinning shaft bi-simply supported as a function of rotating speed Ω (Campbell diagram) for various ratios e/D. It is the same spinning shaft used previously (D =0.1m).

In spite of the change of the e/D ratio, the first natural frequencies are slightly increased. This is due to the deformation of the cross section is negligible, and thus natural frequencies of the thin-walled shaft would approximately independent of thickness ratio e/D.

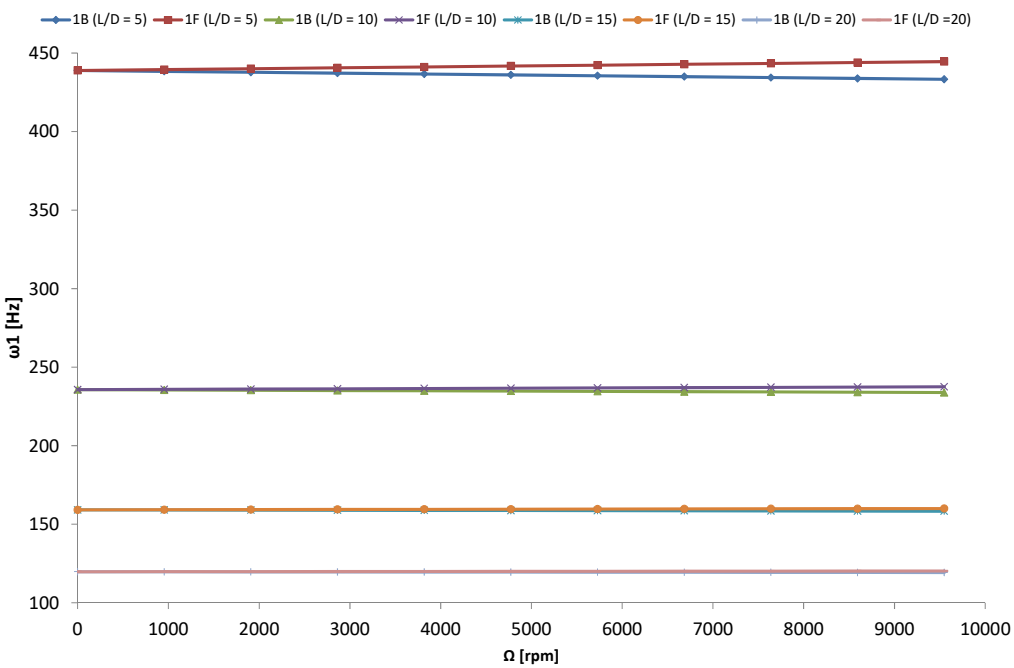

Figure 10: Campbell diagram for the bending fundamental frequency ω_1 of the carbon- epoxy shaft bi-simply supported for various ratios L/D.

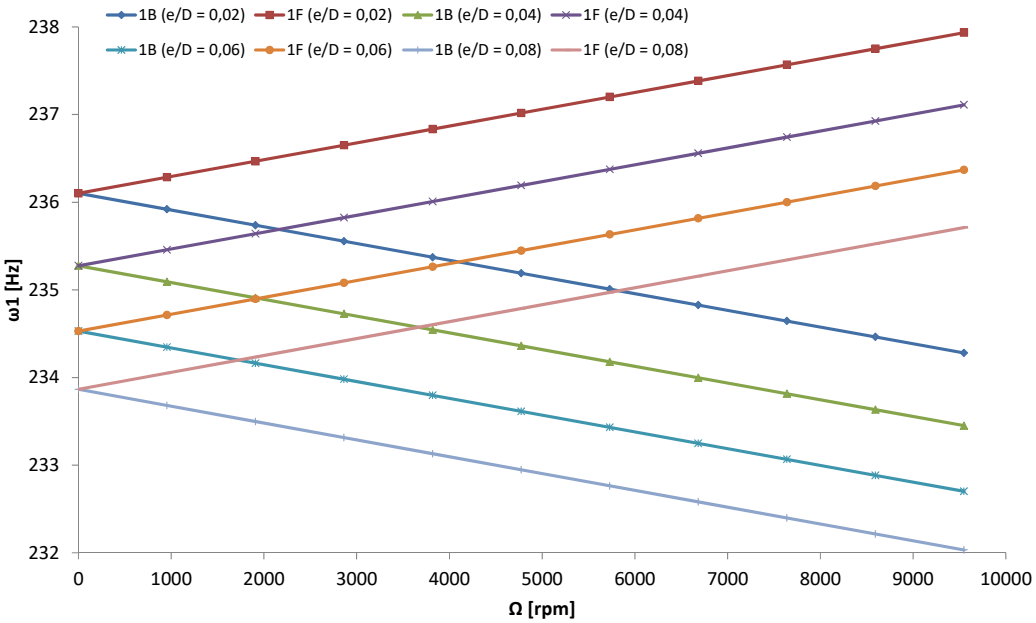

Figure 11: Campbell diagram for the bending fundamental frequency ω_1 of the carbon- epoxy spinning shaft bi-simply supported for various ratios e/D.

4 CONCLUSIONS

The free vibrations analysis of spinning composite shafts with curvilinear fibers using the p-version of finite element method with trigonometric shape functions is presented in this analysis. In the absence of data on vibrations of spinning composite shafts with curvilinear fibers, the formulation is verified by comparisons with published data on spinning composite shafts reinforced by straight fibers.The results obtained agree with those available in the literature. Several examples were treated to determine the influence of the various geometrical and mechanical parameters of the spinning shafts on natural frequencies. This work use led to obtain at the following conclusions

- Monotonous and uniform convergence is checked by increasing the number of the shape functions p. The convergence of the solutions is ensured by the element beam with two nodes. The results agree with the solutions found in the literature.
- The gyroscopic effect causes a coupling of orthogonal displacements to the axis of rotation, and by consequence separates the frequencies in two branches, backward (B) and forward (F) precession modes. In all cases the forward modes increase with increasing rotating speed however the backward modes decrease. This effect has a significant influence on the behaviors of the spinning shafts.
- The first natural frequencies of the thin-walled spinning composite shaft are approximately independent of the thickness ratio and mean diameter of the shaft.
- The first bending natural-frequencies of the spinning composite shafts are influenced appreciably by changing the ply angle $\eta\,(x)$ of curvilinear fibers, the stacking sequence, the length, the mean diameter, the materials, the rotating speed and the boundary conditions.

– If we combine the same fiber orientations to form various stackings, we find:
  (a) The first bending natural-frequencies are almost the same if we permute the angles T_0 and T_1 in the same layer and are very close if we permute two adjacent layers.
  (b) The first bending natural-frequencies of spinning shafts which have anti-symmetric stackings are very close and are a little close which have symmetric stackings.
  (c) The first bending natural-frequencies of spinning shafts which have unsymmetric stackings are far.

Prospects for studies which can be undertaken following this work: Curvilinear fiber optimization of a spinning composite shaft.

References

Abdalla, M.M., Setoodeh, S., Gürdal, Z. (2007). Design of variable stiffness composite panels for maximum fundamental frequency using lamination parameters. Composite Structures 81(2): 283-291.

Bert, C.W., Kim, C.D. (1995). Whirling of composite-material driveshafts including bending, twisting coupling and transverse shear deformation. Journal of Vibration and Acoustics 117: 17-21

Berthelot, J.M. (1996). Matériaux Composites, Comportement Mécanique et Analyse des Structures, Masson, Paris, Deuxième édition.

Blom, A.W., Setoodeh, S., Hol, J., Gürdal, Z. (2008).Design of variable-stiffness conical shells for maximum fundamental Eigen frequency. Computers and Structures 86(9): 870–878.

Blom, A.W., Stickler, P.B., Gürdal, Z. (2010). Optimization of a composite cylinder under bending by tailoring stiffness properties in circumferential direction. Composites Part B: Engineering 41(2): 157-165.

Boukhalfa, A. (2014). Dynamic analysis of a spinning functionally graded material shaft by the *p*-version of the finite element method. Latin American Journal of Solids and Structures 11: 2018-2038

Boukhalfa, A., Hadjoui, A. (2010). Free vibration analysis of an embarked rotating composite shaft using the *hp*-version of the FEM. Latin American Journal of Solids and Structures 7: 105–141

Boukhalfa, A., Hadjoui, A., Hamza Cherif, S.M. (2008). Free vibration analysis of a rotating composite shaft using the *p*-version of the finite element method. International Journal of Rotating Machinery. Article ID 752062, 10 pages.

Chang, M.Y., Chen, J.K., Chang, C.Y. (2004). A simple spinning laminated composite shaft model. International Journal of Solids and Structures 41: 637–662.

Dharmarajan, S., McCutchen Jr., H. (1973). Shear coefficients for orthotropic beams. Journal of Composite Materials 7: 530–535.

DiNardo, M.T., Lagace, P.A. (1989). Buckling and postbuckling of laminated composite plates with ply drop-offs. *AIAA journal* 27(10): 1392–1398.

Gürdal, Z., Olmedo R. (1993). In-plane response of laminates with spatially varying fiber orientations-variable stiffness concept. AIAA journal 31(4): 751–758.

Gürdal, Z., Olmedo, R. (1992). Composite laminates with spatially varying fiber orientations: variable stiffness panel concept. Proceedings of the AIAA/ASME/ASCE/AHS/ASC 33rd structures, structural dynamics and materials conference (2): 798–808.

Gürdal, Z., Tatting, B.F., Wu, K.C. (2005).Tow-placement technology and fabrication issues for laminated composite structures. Proceedings of the 46th AIAA/ASME/ASCE/AHS/ASC Structures, Structural Dynamics and Materials (SDM) Conference, Austin TX.

Haddadpour, H., Zamani, Z. (2012). Curvilinear fiber optimization tools for aeroelastic design of composite wings. Journal of Fluids and Structures 33: 180–190

Hyer, M., Charette, R. (1991). Use of curvilinear fiber format in composite structure design. AIAA journal, vol. 29(6):1011–1015.

Hyer, M., Lee, H. (1991). The use of curvilinear fiber format to improve buckling resistance of composite plates with central circular holes. Composite Structures 18(3): 239-261.

Khani, A., IJsselmuiden, S., Abdalla, M., Gürdal, Z. (2011). Design of variable stiffness panels for maximum strength using lamination parameters. Composites Part B: Engineering 42(3): 546-552.

Leissa, A., Martin, A. (1990). Vibration and buckling of rectangular composite plates with variable fiber spacing. Composite Structures 14(4): 339–357.

Marouene, A. (2015). Résistance à la compression et au flambage des composites carbone/époxy à rigidité variable fabriqués par le procédé de placement automatique des fibres, Ph.D. Thesis (in French), Montreal University, Montreal Polytechnic, Canada.

Nik, MA., Fayazbakhsh, K., Pasini, D., Lessard, L. (2012). Surrogate-based multi-objective optimization of a composite laminate with curvilinear fibers. Composite Structures 94(8): 2306-2313.

Olmedo, R., Gürdal, Z. (1993). Buckling response of laminates with spatially varying fiber orientations. Proceedings of the AIAA/ASME/ASCE/AHS/ASC 34th Structures, Structural Dynamics, and Materials Conference (1): 2261–2269.

Ribeiro, P. (2015a). Non-linear modes of vibration of thin cylindrical shells in composite laminates with curvilinear fibres. Composite Structures 122: 184–197

Ribeiro, P. (2015b). Linear modes of vibration of cylindrical shells in composite laminates reinforced by curvilinear fibres. Journal of Vibration and Control: 1–18.

Ribeiro, P., Akhavan, H. (2012). Non-linear vibrations of variable stiffness composite laminated plates. Composite Structures 94(8): 2424-2432.

Ribeiro, P., Akhavan, H., Teter, A., Warmiński, J. (2014). A Review on the mechanical behaviour of curvilinear fibre composite laminated panels. Journal of Composite Materials 48(22): 2761–2777.

Rouhi, M., Ghayoor, H., Hoa, S.V., Hojjati, M. (2015). Multi-objective design optimization of variable stiffness composite cylinders. Composites Part B: Engineering 69: 249-255.

Singh, S.E., Gupta, K. (1996). Composite shaft rotordynamic analysis using a layerwise theory. Journal of Sound and Vibration 191(5):739–756

Tatting, B.F. (1998). Analysis and design of variable stiffness composite cylinders. Ph.D. Thesis, Virginia Polytechnic Institute and State University, USA.

Venkatachari, A., Natarajan, S., Haboussi, M., Ganapathi, M. (2016). Environmental effects on the free vibration of curvilinear fibre composite laminates with cutouts. Composites Part B 88: 131-138.

Waldhart, C. (1996). Analysis of tow-placed, variable-stiffness laminates. Ph.D. Thesis, Virginia Polytechnic Institute and State University, USA.

Wu, Z., Weaver, PM., Raju, G. (2013). Postbuckling optimisation of variable angle tow composite plates. Composite Structures 103: 34-42.

Yazdani, S., Ribeiro, P. (2015). A layerwise *p*-version finite element formulation for free vibration analysis of thick composite laminates with curvilinear fibres. Composite Structures 120: 531–542

Zamani, Z., Haddadpour, H., Ghazavi, M.R. (2011). Curvilinear fiber optimization tools for design thin walled beams. Thin-Walled Structures 49: 448–454.

NOMENCLATURE

$U(x, y, z)$	Displacement in x direction.
$V(x, y, z)$	Displacement in y direction.
$W(x, y, z)$	Displacement in z direction.
β_x	Rotation angles of the cross-section about the y axis.
β_y	Rotation angles of the cross-section, about the z axis.
ϕ	Angular displacement of the cross-section due to the torsion deformation of the shaft.
E	Young modulus.
G	Shear modulus.
(1, 2, 3)	Principal axes of a layer of laminate
$\left(\vec{i}, \vec{e}_r, \vec{e}_\theta\right)$	Axes of cylindrical coordinates.
$\left(\vec{i}, \vec{j}, \vec{k}\right)$	Axes of Cartesian coordinates.
(x, y, z)	Cartesian coordinates.
(x, r, θ)	Cylindrical coordinates.
$C_{ij}^{'}, C_{ij}$	Elastic constants.
k_s	Shear correction factor.
ν	Poisson coefficient.
ϱ	Masse density.
L	Length of the shaft.
D	Mean radius of the shaft.
e	Wall thickness of the shaft.
R_n	The nth layer inner radius of the composite shaft.
R_{n+1}	The nth layer outer radius of the composite shaft.
k	Number of the layer of the composite shaft.
$\eta(x)$	Lamination angle of curvilinear fibers.
θ	Circumferential coordinate.
ξ	Local and non-dimensional co-ordinates.
ω	Natural frequency
Ω	Rotating speed.
$[N]$	Matrix of the shape functions.
$f(\xi)$	Shape functions.
p	Number of the shape functions or number of hierarchical terms.
t	Time.
E_c	Kinetic energy.
E_d	Strain energy.
$\{q_i\}$	Generalized coordinates, with $(i = U, V, W, \beta_x, \beta_y, \phi)$
$[M]$	Masse matrix.
$[K]$	Stiffness matrix.
$[G]$	Gyroscopic matrix.
T_0, T_1	Angles of curvilinear fibers.

APPENDIX

The various matrices of the equation (14) as follows:

$$[M]=\begin{bmatrix}[M_U] & 0 & 0 & 0 & 0 & 0\\ 0 & [M_V] & 0 & 0 & 0 & 0\\ 0 & 0 & [M_W] & 0 & 0 & 0\\ 0 & 0 & 0 & [M_{\beta_x}] & 0 & 0\\ 0 & 0 & 0 & 0 & [M_{\beta_y}] & 0\\ 0 & 0 & 0 & 0 & 0 & [M_\phi]\end{bmatrix};\ [K]=\begin{bmatrix}[K_U] & 0 & 0 & 0 & 0 & [K_1]\\ 0 & [K_V] & 0 & [K_2] & [K_3] & 0\\ 0 & 0 & [K_W] & [K_4] & [K_5] & 0\\ 0 & [K_2]^T & [K_4]^T & [K_{\beta_x}] & [K_6] & 0\\ 0 & [K_3]^T & [K_5]^T & [K_6]^T & [K_{\beta_y}] & 0\\ [K_1]^T & 0 & 0 & 0 & 0 & [K_\phi]\end{bmatrix} \quad \text{(A1-2)}$$

$$[G]=\begin{bmatrix}0&0&0&0&0&0\\0&0&0&0&0&0\\0&0&0&0&0&0\\0&0&0&0&[G_1]&0\\0&0&0&-[G_1]^T&0&0\\0&0&0&0&0&0\end{bmatrix};\quad [M_U]=I_m L\int_0^1 [N_U]^T[N_U]\,d\xi\ ;\qquad [M_V]=I_m L\int_0^1 [N_V]^T[N_V]\,d\xi \quad \text{(A3-4-5)}$$

$$[M_W]=I_m L\int_0^1 [N_W]^T[N_W]\,d\xi\ ;\ [M_{\beta_x}]=I_d L\int_0^1 [N_{\beta_x}]^T[N_{\beta_x}]\,d\xi\ ;\ [M_{\beta_y}]=I_d L\int_0^1 [N_{\beta_y}]^T[N_{\beta_y}]\,d\xi \quad \text{(A6-7-8)}$$

$$[M_\phi]=I_p L\int_0^1 [N_\phi]^T[N_\phi]\,d\xi\ ;\quad [K_U]=\frac{1}{L}\int_0^1 A_{11}[N'_U]^T[N'_U]\,d\xi\ ;\quad [K_V]=\frac{1}{L}k_s\int_0^1 (A_{55}+A_{66})[N'_V]^T[N'_V]\,d\xi \quad \text{(A9-10-11)}$$

$$[K_W]=\frac{1}{L}k_s\int_0^1 (A_{55}+A_{66})[N'_W]^T[N'_W]\,d\xi\ ;\ [K_1]=\frac{1}{L}k_s\int_0^1 A_{16}[N'_\phi]^T[N'_U]\,d\xi \quad \text{(A12-13)}$$

$$[K_2]=-\frac{1}{2L}k_s\int_0^1 A_{16}[N'_V]^T[N'_{\beta_x}]\,d\xi\ ;\qquad [K_3]=-k_s\int_0^1 (A_{55}+A_{66})[N_{\beta_y}]^T[N'_V]\,d\xi \quad \text{(A14-15)}$$

$$[K_4]=k_s\int_0^1 (A_{55}+A_{66})[N_{\beta_x}]^T[N'_W]\,d\xi\ ;\qquad [K_5]=-\frac{1}{2L}k_s\int_0^1 A_{16}[N'_W]^T[N'_{\beta_y}]\,d\xi \quad \text{(A16-17)}$$

$$[K_6]=\left[\frac{1}{2}k_s\int_0^1 A_{16}[N_{\beta_y}]^T[N'_{\beta_x}]\,d\xi\right]-\left[\frac{1}{2}k_s\int_0^1 A_{16}[N_{\beta_x}]^T[N'_{\beta_y}]\,d\xi\right];\ [K_\phi]=\frac{1}{L}k_s\int_0^1 B_{66}[N'_\phi]^T[N'_\phi]\,d\xi \quad \text{(A18-19)}$$

$$[K_{\beta_x}]=\left[\frac{1}{L}\int_0^1 B_{11}[N'_{\beta_x}]^T[N'_{\beta_x}]\,d\xi\right]+\left[Lk_s\int_0^1 (A_{55}+A_{66})[N_{\beta_x}]^T[N_{\beta_x}]\,d\xi\right];\ [G_1]=\Omega I_p L\int_0^1 [N_{\beta_x}]^T[N_{\beta_y}]\,d\xi \quad \text{(A20-21)}$$

$$[K_{\beta_y}]=\left[\frac{1}{L}\int_0^1 B_{11}[N'_{\beta_y}]^T[N'_{\beta_y}]\,d\xi\right]+\left[Lk_s\int_0^1 (A_{55}+A_{66})[N_{\beta_y}]^T[N_{\beta_y}]\,d\xi\right] \quad \text{(A22)}$$

The terms of the matrices are a function of the integrals: $J_{mn}^{\alpha\beta}=\int_0^1 f_m^\alpha(\xi)\,f_n^\beta(\xi)\ \ d\xi$; $(m,\ n)$ indicate the number of the shape functions used, and (α,β) is the order of derivation.